New Journal of Physics
The open access journal at the forefront of physics

Deutsche Physikalische Gesellschaft DPG IOP Institute of Physics

FAST TRACK COMMUNICATION • OPEN ACCESS

Nonlinear patterns shaping the domain on which they live

New Journal of Physics
The open access journal at the forefront of physics

Deutsche Physikalische Gesellschaft DPG
IOP Institute of Physics

Published in partnership with: Deutsche Physikalische Gesellschaft and the Institute of Physics

OPEN ACCESS

RECEIVED
10 December 2019

REVISED
5 March 2020

ACCEPTED FOR PUBLICATION
12 March 2020

PUBLISHED
5 May 2020

FAST TRACK COMMUNICATION

Nonlinear patterns shaping the domain on which they live

Mirko Ruppert[1], **Falko Ziebert**[2,3] and **Walter Zimmermann**[1]

[1] Theoretische Physik I, Universität Bayreuth, 95440 Bayreuth, Germany
[2] Institute for Theoretical Physics, Heidelberg University, 69120 Heidelberg, Germany
[3] Max Planck Institute for Dynamics and Self-Organization (MPIDS), 37077 Göttingen, Germany

E-mail: walter.zimmmermann@uni-bayreuth.de

Keywords: pattern formation, pattern selection, phase field

Abstract

Nonlinear stripe patterns in two spatial dimensions break the rotational symmetry and generically show a preferred orientation near domain boundaries, as described by the famous Newell–Whitehead–Segel (NWS) equation. We first demonstrate that, as a consequence, stripes favour rectangular over quadratic domains. We then investigate the effects of patterns 'living' in deformable domains by introducing a model coupling a generalized Swift–Hohenberg model to a generic phase field model describing the domain boundaries. If either the control parameter inside the domain (and therefore the pattern amplitude) or the coupling strength ('anchoring energy' at the boundary) are increased, the stripe pattern self-organizes the domain on which it 'lives' into anisotropic shapes. For smooth phase field variations at the domain boundaries, we simultaneously find a selection of the domain shape and the wave number of the stripe pattern. This selection shows further interesting dynamical behavior for rather steep variations of the phase field across the domain boundaries. The here-discovered feedback between the anisotropy of a pattern and its orientation at boundaries is relevant e.g. for shaken drops or biological pattern formation during development.

1. Introduction

Fascinating pattern formation phenomena are ubiquitous in nature [1–4]. Examples include spatially periodic patterns in convection systems from small to geological scales [4–7], surface waves [8] or patterns in biological systems [9–11] down to the scales of single cells, including for instance cell polarization that resembles phase separation [12–14]. Often patterns emerge in finite areas or volumes. While most patterns occur in systems of fixed domain shapes, the action of nonlinear patterns on deformable domains they 'live on' has attracted increasing attention only recently [15–17]. Here, we hence address the following fundamental question: how do nonlinear stripe patterns affect in a generic manner the shape of a domain with deformable boundaries on which they form?

In finite domains, the effects of boundaries become important. They influence, for instance, the orientation and the wavelength of spatially periodic patterns [5, 18–23]. For the well-studied case of thermal convection, an isotropic system, the convection rolls orient perpendicular to the vertical container walls due to the (no-slip) boundary condition for the flow field [21–23]. In general, for intrinsic isotropic systems a vanishing pattern amplitude, imposed by boundary conditions, leads to an orientation of stripes perpendicular to the boundaries [5, 19]. They may additionally restrict the range of the pattern's wave numbers that are stable and hence observable [20].

Importantly, apart from real boundaries, the emergence of patterns can be restricted to finite domains also via restricting the forces driving the pattern formation process to be sufficiently strong (i.e. supercritical) only in a subdomain of a larger system. Examples are pattern forming light-sensitive chemical reactions [24], *in vitro* protein reactions on membranes [25] or again fluid systems [26–28]. In these cases, no specific boundary conditions act on the concentration or flow fields that will become patterned but

rather the control parameter drops from super- to subcritical values outside of a certain domain. Such spatial restrictions have been so far mostly studied in quasi one-dimensional systems. There, smooth control parameter drops may strongly narrow the wavenumber band of stable periodic patterns or may even select a specific wave number out of it [26, 28, 29], while rapid drops can cause pinning effects [30]. There are recent indications that in two-dimensional systems, control parameter drops can have orientational effects on stripe patterns, similar to 'real' boundary conditions [31].

Orientation effects for patterns at boundaries are closely related to the important fact that the emergence of a stripe pattern in two spatial dimensions breaks the rotational symmetry of the respective system. Here we ask the important question: if we consider domains with flexible boundaries, will the spontaneous symmetry breaking effect of pattern formation lead to a preference of anisotropic shapes of domains in which a stripe pattern forms? On general grounds, it is a completely unexplored question whether, and if so how, finite amplitude patterns can act—via their universal properties—as a means to shape the domains on which they 'live'. There exist, however, experimental example systems. If—naturally very deformable—liquid drops are placed on a surface and are shaken vertically, the so-called Faraday instability causes oscillating, spatially periodic stripe patterns at the drop's free surface [8]. Experiments [15, 16] and simulations [32] show that with increasing amplitude of the Faraday waves, the liquid drops of originally circular cross-section (their three-dimensional shape being a spherical cap) deform to elliptical and finally even worm-like shapes. Is this a general effect for patterns in deformable domains? If so, it would be highly relevant for biology, where both single cells and whole organisms have to become both internally structured and elongated ('polarized') by the intricately regulated interplay of, typically biochemical, patterning and elastic deformations, the most important examples being cell division and symmetry breaking in development [33]. Finally, understanding the generic properties of the 'self-shaping' of 'active domains' may also give insights for the development of biomimetic approaches along the lines of, e.g. [25].

2. Stripe patterns favour rectangular domains

Let us first recall the orientation of nonlinear stripe patterns with respect to boundary conditions in fixed domains and demonstrate why stripes prefer rectangular, i.e. anisotropic domains. We choose the Swift–Hohenberg (SH) model, known to capture the generic features of stationary stripe patterns [5, 19, 34],

$$\partial_t u = \left[\beta - (q_0^2 + \nabla^2)^2\right] u - au^3 - bu(\nabla u)^2. \tag{1}$$

This equation for $u(x, y, t)$ is isotropic in the x–y-plane and $\pm u$ symmetric. q_0 is the preferred dimensionless wave number of stripe solutions. These evolve for positive values of the control parameter, $\beta > 0$. Their amplitude is limited by the cubic nonlinearities for $a > 0, b \geqslant 0$ (supercritical bifurcation).

For $b = 0$ equation (1) is the common SH-model and follows a gradient dynamics, $\partial_t u = -\frac{\delta \mathcal{F}_u}{\delta u}$, with the functional

$$\mathcal{F}_u = \frac{1}{2}\int \mathrm{d}x\,\mathrm{d}y \left[-\beta u^2 + \frac{a}{2}u^4 - \left(\left(q_0^2 + \nabla^2\right) u\right)^2\right]. \tag{2}$$

For $b \neq 0$ equation (1) is a generalization of the original SH model and includes non-potential effects [19]. The model was studied in reference [19] in rectangular domains R with $u = \partial_n u = 0$ along the boundaries ∂R, where ∂_n denotes the derivative normal to the boundaries. In this case, stripe patterns prefer to orient perpendicularly to the boundary. Moreover, if the control parameter β in equation (1) varies from a supercritical value inside a certain domain ($\beta > 0$) to a subcritical value outside ($\beta < 0$), e.g. as specified below in equation (7), the stripes also preferably orient perpendicular to this 'effective boundary'. This is in agreement with results obtained for convection rolls in temperature-field ramps [35] and with studies of turing patterns [31] near non-resonant control parameter ramps.

The—completely generic—orientation of stripe patterns near boundaries can be understood as follows. A supercritically bifurcating spatially periodic pattern (with equation (1) just being a representative) with wave vector $\mathbf{q}_0 = (q_0, 0)$ can be decomposed into a rapidly varying part $\exp(iq_0x)$ and a complex envelope $A(x, y, t)$, which is slowly varying on the length scale $\lambda = 2\pi/q_0$ [2, 5, 36]. The envelope A follows the Newell–Whitehead–Segel equation (NWSE) that covers the major properties of stripe patterns close to threshold (including also the non-gradient case of equation (1) with $b \neq 0$). Importantly, the NWSE also follows a gradient dynamics [2, 5]

$$\tau_0 \partial_t A = -\frac{\delta F}{\delta A^*}, \quad \text{with}$$
$$\mathcal{F}_A = \frac{1}{2}\int \mathrm{d}x\,\mathrm{d}y \left[-\epsilon|A|^2 + \frac{g}{2}|A|^4 + \left| \xi_0 \left(\partial_x - \frac{\mathrm{i}}{2q_0}\partial_y^2 \right) A \right|^2 \right]. \tag{3}$$

We note that if the NWSE is derived from the dimensionless equation (1), one has $\tau_0 = 1$, $\varepsilon = \beta$, $g = 3a + q_0^2 b$ and $\xi_0 = 2q_0$.

Since its dynamics is relaxational, on sufficiently large domains R the NWSE has constant solutions $A_{\mathrm{hom}} = \pm\sqrt{\varepsilon/g}$ in the bulk. What about the boundaries? According to the different orders of the derivatives along the x and y-axis, the NWSE is anisotropic. By replacing $x \to x/l_p$ and $y \to y/l_n$ with

$$l_n = \frac{\xi_0}{\sqrt{\varepsilon}}, \quad \text{and} \quad l_p = \left(\frac{\xi_0^2}{4q_0^2\varepsilon} \right)^{1/4}, \tag{4}$$

and rescaling time and amplitude in the NWSE the coefficients in this equation have all the value '1'. Hence, for a stripe pattern with wave vector $\mathbf{q}$ oriented normally (respectively parallely) to the domain boundary ∂R, its amplitude A decays to zero on a length scale $\propto l_n$ (respectively $\propto l_p$), see also appendix B. Since the NWSE evolves towards the minimum of the functional $\mathcal{F}_A$, a stripe pattern prefers to stay at its bulk value A_{hom} for a maximum possible area. Hence, due to the relation $l_p < l_n$ for the decay along the boundaries, the wave vector $\mathbf{q}$ preferentially aligns parallel to the interface and consequently the stripe pattern perpendicular to it.

Let us assume a fixed, rectangular area $R = L_x L_y$ with aspect ratio $\Gamma = L_x/L_y$ and hence $L_y = \sqrt{R/\Gamma}$. In the bulk, the stripe pattern has amplitude $A \propto \sqrt{\varepsilon/g}$ and $\mathcal{F}_A \propto \varepsilon^2 R$. In the case of the boundary condition $A = 0$ along ∂R, or a control parameter ramp [31], the pattern decays across ∂R on the length scale l_n or l_p, depending on the orientation. With these lengths, and the approximation that at the interfaces the functional is on average halved, the functional for the domain is proportional to

$$\mathcal{F}_A \propto -\varepsilon^2 \left(R - l_n L_y - l_p L_x \right) \tag{5}$$

with a minimum at a finite aspect ratio $\Gamma_{\min} = \left(4q_0^2\xi_0^2/\varepsilon\right)^{1/4}$. The minimum as a function of Γ occurs, since large aspect ratios are again unfavorable for the following reason: for narrow rectangles with a width becoming of the order of a few l_p, the stripes amplitude is suppressed, i.e. cannot reach the bulk value anymore.

Therefore, a stripe pattern near threshold has a lower value of the functional $\mathcal{F}_A$ on rectangular domains $L_y > L_x$ than on a square domain, at fixed area of the domain. This scaling result for supercritically bifurcating stripe patterns in finite domains is universal and holds besides many systems described by the NWSE [5] also for equation (1) and $b \neq 0$. We confirmed this result by simulating equation (1) in the case of gradient dynamics ($b = 0$) and a control parameter defined as

$$\beta(x, y) = \varepsilon(2\rho(x, y) - 1) \tag{6}$$

with

$$\rho(x, y) = \frac{1}{4}\left[\tanh\left(\frac{x + \frac{L_x}{2}}{\sqrt{\xi_\beta}} \right) - \tanh\left(\frac{x - \frac{L_x}{2}}{\sqrt{\xi_\beta}} \right) \right] \times \left[\tanh\left(\frac{y + \frac{L_y}{2}}{\sqrt{\xi_\beta}} \right) - \tanh\left(\frac{y - \frac{L_y}{2}}{\sqrt{\xi_\beta}} \right) \right] \tag{7}$$

to implement a supercritical control parameter in the range $[-L_x/2, L_x/2] \times [-L_y/2, L_y/2]$ with the domain area $R = L_x L_y$.

Keeping the size R of the domain fixed we determined the stationary solutions of equation (1) for different values of $\Gamma = L_x/L_y$ and the respective values of the functional $\mathcal{F}_u$. The result for the functional is shown in figure 1 as a function of Γ for different values of ε. These numerical results confirm the scaling estimate from above, i.e. that for stripe patterns the functional in equation (2) has a minimum for finite aspect ratios $\Gamma > 1$ of the domain. This line of arguments strongly suggests that stripe patterns will favor anisotropic domains if the boundaries of their domain are movable or deformable by the pattern. We will investigate this feedback of a pattern on its domain in the following sections in more detail.

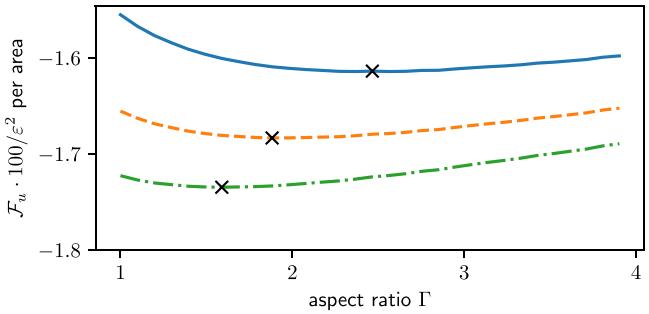

Figure 1. The (scaled) functional $\mathcal{F}_u$ in equation (2) as a function of the aspect ratio $\Gamma = L_x/L_y$ at fixed area $R = L_xL_y$. $\mathcal{F}_u$ has been evaluated for stationary stripe solutions of equation (1) for $b = 0$, using the control parameter ramps as given by equation (7) and for three values of ε: $\varepsilon = 0.1$ (solid blue line), 0.2 (dashed orange line) and 0.4 (dashed-dotted green line). Crosses mark the minimum of $\mathcal{F}_u$. Other parameters: $\xi_\beta = 8$, $a = 1$, $q_0 = 1$ and $b = 0$.

3. Coupling of stripe patterns to deformable domain boundaries

A deformable finite domain R with a positive control parameter inside and a negative one outside can be elegantly implemented by the so-called phase field method. This approach, originally developed for solidification processes [37] has been applied in recent years to many soft matter [38] and biological problems [39], for instance droplets and vesicles in flows [40] or cell motility [41]. It is a well-adapted approach to self-consistently describe deformable and/or moving boundaries.

The idea is to render the function $\rho(x, y)$, that occurs via equation (6) in the control parameter, dynamic. The phase field $\rho(x, y, t)$ has values $\rho = 1$ inside the given domain R, $\rho = 0$ outside and a diffuse interface in between, the $\rho = 1/2$-isoline being identified with the domain boundary ∂R. The phase field dynamics is over damped,

$$\partial_t \rho = -\frac{\delta \mathcal{F}_\rho}{\delta \rho}, \quad \text{with} \quad \mathcal{F}_\rho = \int \left[f(\rho) + \frac{D_\rho}{2} (\nabla \rho)^2 \right] \mathrm{d}x\, \mathrm{d}y. \tag{8}$$

Herein $f(\rho) = \int_0^\rho (1 - \rho')(\delta - \rho')\rho' \mathrm{d}\rho'$ is the homogeneous energy density, having a double well structure with minima at the 'phases' $\rho = 1, 0$. The gradient term in $\mathcal{F}_\rho$ corresponds to a wall energy penalizing domain walls. D_ρ determines the interface width (which in 1D is given by $2\sqrt{2D_\rho}$) and the effective surface tension (also $\propto \sqrt{D_\rho}$). More complex interfacial properties and feedbacks can be implemented [42], but we here consider only the simplest wall energy. The parameter δ occurring in the energy density is chosen as $\delta = \frac{1}{2} - \mu \left(\int \rho \, \mathrm{d}x \, \mathrm{d}y - R_0 \right)$. $\delta = 1/2$ is the stationary point, where $\rho = 0, 1$ have equal energy and hence flat interfaces are stationary. In fact, in 1D this choice leads to hyperbolic tangent solutions as assumed in equation (7). The second term is a simple implementation of area conservation to a fixed value R_0 with the stiffness of the constraint given by μ (we here use $\mu = 0.1$ throughout). We refer to appendix A for an alternative implementation of an intrinsically conserved phase field, yielding qualitatively the same results as equation (8).

Stripe patterns have a certain stiffness that tries to keep stripes straight and, as described above, they prefer to orient themselves perpendicular to a domain boarder suppressing the patterns amplitude. Accordingly, the intrinsic elasticity of stripe-pattern may cause deformations of a flexible domain boundary, as they are described by the phase field. The preferred perpendicular orientation between domain boundaries and stripe patterns has similarities with the homeotropic (perpendicular) orientation of nematic liquid crystals at container boundaries for which there is a generic mean field description of the coupling between the orientation of nematic liquid crystals and the container boundaries [43]. Translating to our case, the orientation of the stripe pattern can be described by the direction of the patterns wave vector, which is parallel to $\nabla u(\mathbf{r}, t)$, and the orientation of the deformable domain boundary by its normal $\nabla \rho$. Accordingly we add to the phase-field potential such a generic orientational contribution

$$\mathcal{F}_\rho^{\text{coupled}} = \mathcal{F}_\rho + \int \frac{\alpha}{2} (\nabla \rho \cdot \nabla u)^2 \, \mathrm{d}x \, \mathrm{d}y, \tag{9}$$

which leads to a feedback of the pattern on the domain shape and favours (vanishes for) the stripe's wave vector perpendicular to the boundary normal. Any other relative orientation costs energy with the stripe orientation parallel to the domain boundary the most costly. The parameter α describes the coupling strength. We note that the phase field acts back on the pattern field u only via the spatial variation of the control parameter given by equation (6).

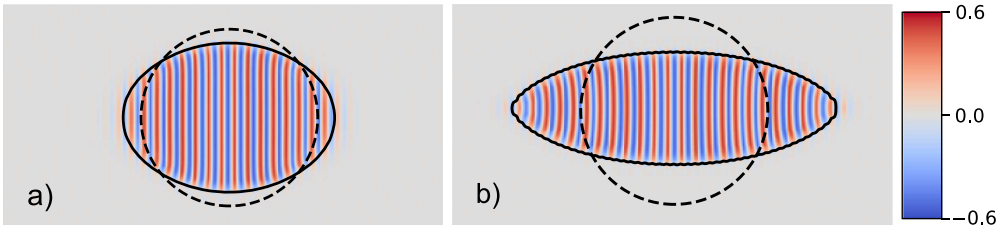

Figure 2. Shown are two stationary solutions of equations (10) that have been obtained starting with a circular initial domain R (marked dashed) and for a supercritical control parameter $\varepsilon = 0.2$. The coupling strength $\alpha = 6$ in (a) leads to a final domain shape with aspect ratio $\Gamma = 1.4$; the value $\alpha = 100$ in (b) to $\Gamma = 2.8$. Other parameters: $D_\rho = 1$, $R_0 = \pi r_0^2$ with $r_0 = 43$; $q_0 = 1$, $a = 1$, $b = 0$.

The final generic model equations for a stripe pattern forming inside a deformable domain then read

$$\begin{aligned} \partial_t \rho &= D_\rho \nabla^2 \rho - (1-\rho)(\delta - \rho)\rho + \alpha \nabla \cdot ([\nabla \rho \cdot \nabla u] \nabla u)\,, \\ \partial_t u &= \left[\varepsilon(2\rho - 1) - (q_0^2 + \nabla^2)^2\right] u - a u^3 - b u (\nabla u)^2, \end{aligned} \tag{10}$$

supplemented by the volume constraint δ as given above.

4. Stripe patterns within deformable domains

Starting simulations of the coupled model equation (10) with circularly shaped domains and with small initial amplitudes for the stripes, we observe a rapid saturation of the stripe amplitude $\propto \sqrt{\varepsilon}$ in the bulk of the domain. After this initial phase of fast dynamics, the finite amplitude stripe pattern starts to deform the flexible domain on a much slower time scale, according to the coupling parameterized by α. An initially circularly shaped domain gets increasingly elongated to an elliptical shape by increasing the coupling parameter α, as indicated in figure 2. In fact, due to this deformation of the domain, stripes can meet the domain boundaries perpendicularly in a larger region. The elongation to elliptical shapes saturates at an aspect ratio $\Gamma > 1$, as we already anticipated from the minimum of $\mathcal{F}_u$ at $\Gamma > 1$ for fixed rectangular domains in figure 1. As indicated in figure 2, the final value of Γ increases with coupling strength α from $\Gamma = 1.4$ at $\alpha = 6$ in part (a) to $\Gamma = 2.8$ for $\alpha = 100$ in part (b). It should also be noted that the deformed domains allow the pattern forming system to fit in additional stripe units, i.e. wavelengths: for the example shown in figure 2(b) from 14 within the circular domain to 24 stripe units.

As indicated in the introduction and in reference [31], rapid and smooth control parameter variations have different effects on patterns and its orientations. In the generic model presented here, the control parameter is directly slaved to the phase field interface. We now study both cases in more depth. We start with the smooth interface case, for which $D_\rho = 1$ as chosen for figure 2 is a good representative.

4.1. Smooth diffuse interfaces

How do pattern forming systems with deformable domains reach their stationary state in this case? We started simulations (with $b = 0$) for different initial aspect ratios, namely with $\Gamma = 1$ below and with $\Gamma = 3$ beyond the final stationary value of Γ. We determined $\mathcal{F}_u(t)$ and $\Gamma(t)$ as a function of time and show $\mathcal{F}_u$ versus Γ in figure 3(a) for three different values of the control parameter ε and for $\alpha = 6$. The bullets ($\bullet$) in each part of the figure mark the final stationary state. Note that this state does not correspond to the minimum of $\mathcal{F}_u(\Gamma)$ (marked by $\times$), since $\mathcal{F}_u$ is not a potential for the full coupled dynamics, only for the pattern formation part. In other words, $\mathcal{F}_u(\Gamma)$ does not reach its minimum, because the system reaches a stationary state as soon as the surface tension-like forces induced by the deformation of the domain and inherent to the phase field description balance the elongational forces induced by the energy gain of orienting the stripes perpendicularly to the domain boundary.

Since the driving force for the deformation of the domain increases with increasing stripe amplitude $\propto \sqrt{\varepsilon}$, also the aspect ratio Γ at the stationary state (marked by $\bullet$) increases with ε. On the other hand the minimum of $\mathcal{F}_u$ (marked by $\times$) decreases with increasing ε and the mismatch between both decreases. Note that, for particular parameters, here for $\varepsilon = 0.4$, the stationary state and the minimum can coincide as indicated in figure 3(a). We find an analogous behavior in figure 3(b), where the control parameter was

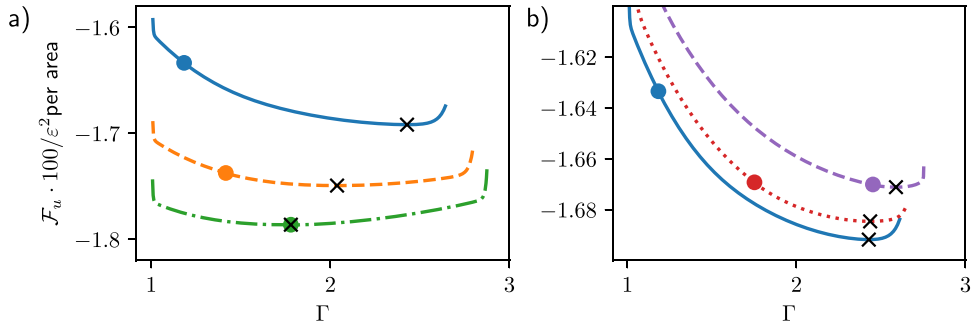

Figure 3. Shown is the rescaled functional $\tilde{\mathcal{F}}_u = \mathcal{F}_u 100/\varepsilon^2$ per unit area for a stripe pattern as a function of the aspect ratio Γ of the domain. The simulation was either started with a circular domain of aspect ratio $\Gamma = 1$ or an elliptical domain with $\Gamma = 3$. In (a) $\tilde{\mathcal{F}}$ and Γ where calculated as a function time for $\alpha = 6$ and for different values of ε: $\varepsilon = 0.1$ (solid blue line), $\varepsilon = 0.2$ (dashed orange line), $\varepsilon = 0.4$ (dashed-dotted green line). The bullets (•) mark the final stationary solution, the crosses (×) the minimum of $\tilde{\mathcal{F}}_u$. Note that the bullet for the dashed line corresponds to the final solution shown in figure 2(b). Part (b) shows a similar plot for a fixed control parameter $\varepsilon = 0.1$ and three values of the coupling strength: $\alpha = 6$ (solid blue line), $\alpha = 30$ (dotted red line) and $\alpha = 100$ (dashed purple line). Further parameters: $D_\rho = 1$, $a = 1$, $b = 0$, $A = r_0^2\pi$, $r_0 = 43$.

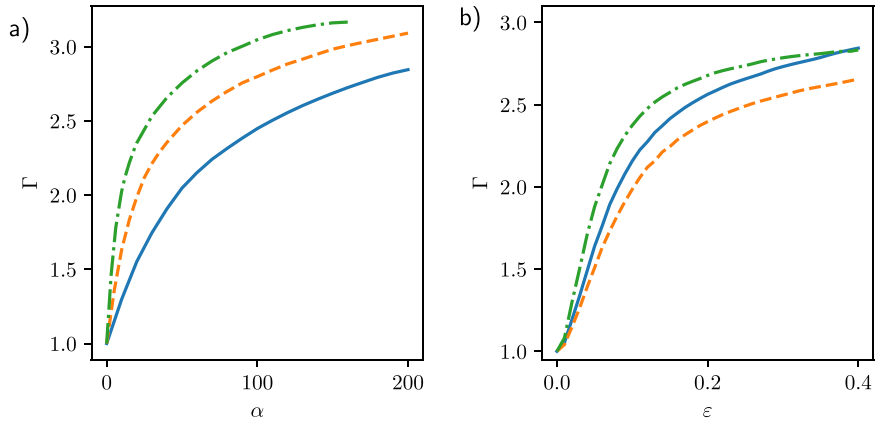

Figure 4. Part (a) shows the aspect ratio Γ as a function of the coupling strength α for three different values of the control parameter: $\varepsilon = 0.1$ (solid blue line), $\varepsilon = 0.2$ (dashed orange line) $\varepsilon = 0.4$ (dashed dotted green line) ($a = 1, b = 0$). Part (b) shows Γ as a function of the control parameter for coupling strength $\alpha = 60$ and three combinations of the nonlinear coefficients: $a = 1, b = 0$ (solid blue line; corresponding to gradient dynamics), $a = 1, b = 1$ (dashed orange line), $a = \frac{1}{3}$, $b = 1$ (dashed dotted green line). Further parameters are: $D_\rho = 1$, $A = r_0^2\pi$, $r_0 = 43$.

fixed and the coupling strength α was varied: again a stronger effect of the pattern on the boundary by increasing the coupling strength reduces the difference between the steady state value of Γ (at •) and the corresponding minimum of $\mathcal{F}_u(\Gamma)$ (marked by ×).

In figure 4 we further quantify how a stripe pattern deforms its domain as function of the parameters. Figure 4(a) shows the final aspect ratio Γ as a function of the coupling strength α for different values of the control parameter ε and at fixed domain area R. The slope of the curves $\Gamma(\alpha)$ increases with ε, but the three curves tend to saturate as a function of α at an upper limit of about $\Gamma_{\max} \sim 3$. This saturation depends essentially on the ratio between the short axis of the ellipse and the decay length l_p. Accordingly, the maximum stationary value of the aspect ratio $\Gamma_{\max}$ will increase with the area R of the domain.

Figure 4(b) shows the final aspect ratio as a function of the control parameter ε for a fixed coupling strength $\alpha = 60$. Here, the solid curve corresponds to the case $b = 0$, exclusively studied so far, corresponding to the case where equation (1) follows a gradient dynamics governed by equation (2). Both the dashed and the dash-dotted curves have been obtained for the non-potential case ($b \neq 0$).

According to figure 4 the effect of the pattern on the boundary, as reflected by the aspect ratio Γ, increases with both the coupling strength α and the pattern amplitude (respectively ε), before it reaches a saturation level. Moreover, these parameter trends are quite similar for the case of gradient and non-gradient dynamics. The pattern deforming its boundary to reduce the functional $\mathcal{F}_u$ is equivalent to its

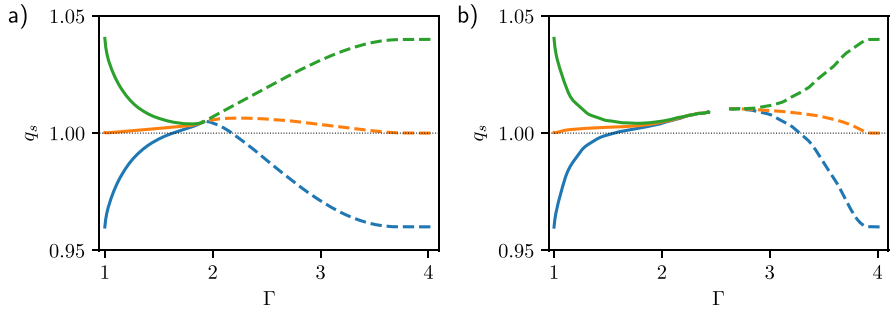

Figure 5. Shown is the time evolution of the wave number $q_s(t)$ of stripe patterns and the aspect ratio $\Gamma(t)$ of the domain in the plane q_s vs Γ. Simulations of equation (10) with $a = 1, b = 0$ were started either with a circularly shaped domain, $\Gamma = 1$ (solid lines), or with a strongly elliptically shaped domain, $\Gamma = 4$ (dashed lines). In both cases, stripe patterns of three different initial wave numbers $q_{\text{init}} = 0.96$ (blue), $q_{\text{init}} = 1.0$ (orange) and $q_{\text{init}} = 1.04$ (green) were studied. In part (a) a smooth, diffuse interface was implemented via $D_\rho = 1$. In (b) $D_\rho = 0.4$ was used, implying a steeper decay of the control parameter.

attempt to reach maximum amplitude in an as large as possible subdomain of R. This trend still holds in the case of a non-gradient dynamics, where it again is achieved best with the stripe pattern staying perpendicularly to the domain boundary.

4.2. Dynamical selection of aspect ratio and wave number

Both the aspect ratio Γ of the domain and the wave number q of the periodic pattern are dynamically selected, as shown in figure 5(a) for the case of a smooth, diffuse control parameter variation across the boundary, using $D_\rho = 1$. In order to demonstrate this statement, we started two sets of simulations of equation (10): on the one hand, we started with a circularly shaped initial domain and a finite amplitude pattern with three different initial wave numbers (solid curves in figure 5(a)). In this case, Γ increases with time until the differently started simulations meet at the same wave number: in fact, the system selects a specific aspect ratio and a specific wave number. On the other hand, we started with periodic patterns of three different wave numbers but now on a domain with a large aspect ratio $\Gamma \sim 4$. Now, Γ decayed with time and again the aspect ratio and the wave numbers evolved to the same value as before. One can hence conclude that the selection process is robust with respect to the initial conditions.

From systems with fixed domain shapes in quasi one-dimension (1D) having smooth spatial parameter variations, the phenomenon of a strong wave-number restriction or selection is well known [26–28]. However, that this behavior also generalizes for deformable two-dimensional systems to a simultaneous selection of the aspect ratio and the wave number, independent of the initial conditions, is rather surprising. In addition, there are two further aspects of wave number selection that are different to previous quasi one-dimensional studies: first, in the quasi 1D case with gradient dynamics the preferred wave number, here $q_0 = 1$, is selected. This corresponds to the wave number where the pattern amplitude takes its maximum as a function of q and the respective functional its minimum (also called the Eckhaus band middle). In contrast, in the 2D deformable domain situation, even in the case of gradient dynamics, the selected wave number $q = 1.005 > q_0 = 1$ does not correspond to the wave number of maximum amplitude or minimum functional.

Second, we note that in the non-gradient case with $b \neq 0$, the amplitude A of a periodic stripe pattern in an extended system (cf $u = Ae^{iqx} + c.c$) is given by

$$A^2 = \frac{\varepsilon - (q_0^2 - q^2)^2}{3a + bq^2}. \tag{11}$$

For $a > 0, b \geqslant 0$, $|A(q)|$ hence should take its maximum at a $q < q_0 = 1$. Nevertheless, in our simulations of equations (10) for $b \neq 0$, we again obtained (not shown) a selected wave number q_s that is larger than q_0 and even larger than the selected wave number in the case of gradient dynamics.

For more rapid and steep control parameter variations across the domain boundary (modeled by smaller values of D_ρ), one still obtains a rather strict wave number selection, as shown in figure 5(b) for $D_\rho < 0.4$. However, the selected stationary aspect ratio depends now on the initial shape, as indicated by the gap in figure 5(b), and on the steepness of the control parameter variation via D_ρ. For smaller values of D_ρ the gap increases. In fact, from quasi-1D systems it is known that more rapid and steep parameter variations may lead via pinning effects to an imperfect wave number selection [30]. We investigate the dynamics in this regime in the next section.

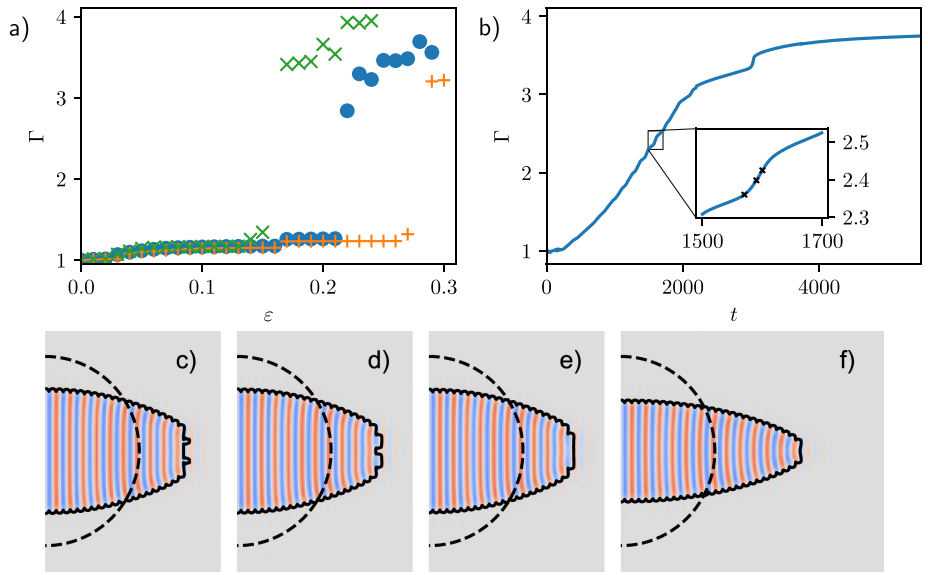

Figure 6. Simulation results for a steep phase field interface ($D_\rho = 0.1$), resulting in a rapid decay of the control parameter across the domain boundary. Panel (a) shows that periodic patterns are pinned for small values of the control parameter ε and the initially circular domain remains essentially undeformed, i.e. the aspect ratio Γ stays close to one. Beyond a critical value of ε, the pattern becomes depinned and Γ increases as indicated by ($\bullet$) for $a = 1, b = 0$, i.e. gradient dynamics, by ($\times$) for $a = 1/3, b = 1$ and by ($+$) for $a = 1, b = 1$. The coupling strength was chosen to be $\alpha = 60$. Panel (b) shows $\Gamma(t)$ for $\varepsilon = 0.2$, $\alpha = 60$ and $a = 1/3, b = 1$. The slight modulations in the curve are a signature of weak pinning effects at the boundary. The snapshots in (c)–(e) illustrate the complex evolution of the pattern during the propagation of the domain boundary at intermediate times, cf crosses in the inset of part (b). Panel (f) displays the stationary final state for the same simulation.

4.3. Steep interfaces and pinning effects

During the evolution from the initially circularly shaped domain to an elliptical domain as exemplified in figure 2(b), new periodic units appear rather smoothly due to the smooth diffuse control parameter variations across the domain boundaries for $D_\rho = 1.0$. When, in contrast, a rather steep phase field variation across the boundary is chosen, as exemplified here by $D_\rho = 0.1$, the periodic pattern may get pinned at the resulting steep control parameter variations. Moreover, the pinning of the stripe pattern may persist over a wide range of control parameters ε, as shown in figure 6(a): for small ε, no further periodic units (wave lengths) can emerge and the aspect ratio Γ stays fixed close to its initial $\Gamma \simeq 1$. Beyond this pinning regime, the pattern rapidly evolves to much larger values of Γ, as shown in figure 6(a) for three different combinations of the nonlinear parameters a, b in equation (10), corresponding to both gradient and non-gradient dynamics.

During this evolution, Γ increases with time as shown exemplarily in figure 6(b). Since the additional periodic units emerge step by step, also the aspect ratio increases in a stepwise fashion, as highlighted by the inset of the same panel. The respective snapshots given in figures 6(c)–(f) illustrate the complex two-dimensional dynamics during the emergence of further periodic units—corresponding to the time $t = 1500$–1700 shown in the inset of figure 6(b)—and, lastly, the finally obtained stationary state.

Note that, while we still found a unique wave-number selection for $D_\rho = 0.4$ in figure 5, this unique selection mechanism does in general not hold anymore for $D_\rho = 0.1$ or smaller.

5. Discussion and conclusion

With the onset of nonlinear stripe patterns in two-dimensional domains, the rotational symmetry is broken. In the often occurring case where the pattern forming field has to vanish outside the domain, this results in an orientational preference for the stripes with respect to domain boundaries. We have shown here that this fundamental property implies that stripe pattern prefer to 'live in' anisotropic domains. This insight then motivated us to study deformable domains. We here applied a generic approach by coupling the Swift–Hohenberg (SH) model to a phase field, describing the deformable domain, and implementing the generic orientational preference of the stripes with respect to the domain boundaries by an energy inspired from surface anchoring of liquid crystals. For both the gradient and a generalized non-gradient version of the SH model we found that increasing either the pattern amplitude or the coupling strength deforms the domain towards elliptical shapes of increasing aspect ratio. The deformation of the domain finally saturates due to two effects: one is related to the fact that with increasing aspect ratio, the short elliptical axis reaches

the range of the coherence length of the pattern along the stripe axis. In this regime the supercritical pattern is prevented to reach its bulk amplitude, which is disfavored. The other effect is the surface or wall energy, inherent to the phase field approach, which resists strong deformations. It should be noted that the latter effect may not be present in some systems, but can also be removed from the phase field dynamics, cf [42, 44].

From the generic modeling point of view, the phase field approach used here has another advantage: the width of its diffuse interface can be tuned via the parameter D_ρ. This allows us to make a connection to previous works on the effects of control parameter ramps in pattern forming systems [26–28]. It is well known that spatially periodic patterns in extended systems are stable for many different wave numbers out of a stable, so-called Eckhaus band [5, 45–47]. In our present study we found the surprising result that the wave number of the pattern and the domain shape described by the aspect ratio are selected *simultaneously*. Furthermore, the selected wave number is larger than the one at the maximum of the amplitude (at the minimum of the potential, in case it exists), irrespective whether the pattern follows gradient dynamics or not. This is different from quasi one-dimensional pattern forming systems, where the wave number at the minimum of the related potential is selected in case of gradient dynamics. Finally, in the case of steep control parameter variations, slightly different domain shapes may be selected depending on initial conditions, and an interesting step-wise dynamics of the domain deformation was observed.

The study of the generic effects of nonlinear stripe patterns in deformable domains undertaken here shares many similarities with the specific example of Faraday waves emerging on top of shaken liquid droplets [15, 16, 32]. However, Faraday waves on droplet surfaces are a three-dimensional situation. As long as the contact area occupied by the drop does not change considerably, our findings should directly apply. For larger drop deformations, the contact area increases and experimentally one finds worm-like droplets and even drop splitting. Such situations could be taken into account within our generic model by considering either three dimensional domains or a slow temporal dynamics for the area.

In conclusion, we studied a generic coupling of stripe patterns to the boundary of the deformable domain wherein they form. Similarly interesting effects may also apply for traveling wave patterns [25, 48]. In addition, in the case of an externally forced boundary motion interesting reorientation effects may occur at a sufficiently high boundary speed [49]. The fact that patterns are generically and inherently coupled to the boundaries/surfaces of the 'domains they live in' should be further investigated, especially in view of biological systems like the growing cells described in references [50, 51] or for the coupling of patterns on interfaces and the domain shape, see e.g. reference [17].

Appendix A. Conserved phase field equation

In the main manuscript, we used an Allen–Cahn approach for the phase field, cf equation (8). The field $\rho(x, y)$ was hence not conserved *a priori*, but area conservation was implemented via the nonlocal term in the definition of the parameter δ.

Another approach is the so-called Cahn–Hilliard model. Here the dynamics of the phase field is explicitly conserved by writing

$$\partial_t \rho = -\nabla^2 \frac{\delta F_\rho}{\delta \rho}. \tag{A.1}$$

Due to the additional spatial derivatives, the model is numerically more involved, but we nevertheless checked here whether the details of the phase field implementation matter for the overall dynamics of patterns in deformable domains.

Using the same potential $\mathcal{F}_\rho^{\text{coupled}}$ as before, but with constant $\delta = \frac{1}{2}$, one arrives at the model equations:

$$\begin{aligned}\partial_t \rho &= -\nabla^2 \left[D_\rho \nabla^2 \rho - (1-\rho)\left(\frac{1}{2} - \rho\right)\rho + \alpha \nabla \cdot ([\nabla \rho \cdot \nabla u]\nabla u) \right], \\ \partial_t u &= \left[\varepsilon(2\rho - 1) - (q_0^2 + \nabla^2)^2\right] u - a u^3 - b u (\nabla u)^2.\end{aligned} \tag{A.2}$$

For finite values of the coupling strength α and positive control parameter ε, this model again prefers an orientation of the stripe pattern perpendicular to the control parameter drop across the interface and elongates the domain as shown in figure A1. The aspect ratio Γ of the stationary elongation increases with both the coupling strength and the control parameter, as shown in figure A2.

Qualitatively, the behavior is identical to the one obtained using the model equation (10). The 'global' domain conservation in model equation (A.2) seems to lead to a stricter compliance with the form of the interface. However, compared to model equation (10), the higher order derivatives in equation (A.2) restricted our study to smaller control parameter values and system sizes.

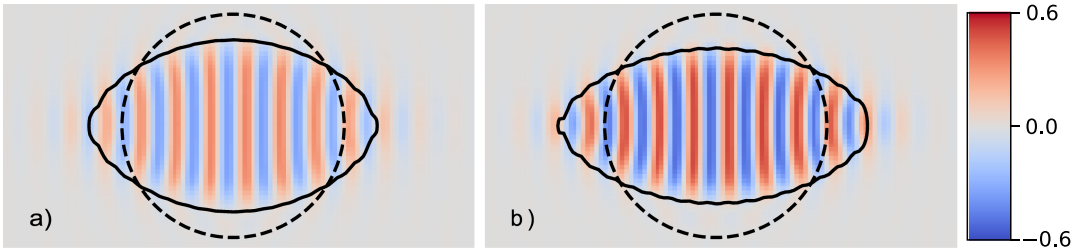

Figure A1. Shown are two stationary solutions of equation (A.2), both with the circular initial domain marked as dashed. The control parameter was chosen to be $\varepsilon = 0.2$ and the coupling strength $\alpha = 6$ in (a) vs $\alpha = 100$ in (b), leading to increasingly deformed domains (solid curves mark the $\rho = 1/2$-isocurves). Other parameters: $D_\rho = 1$, $R_0 = \pi r_0^2$ with $r_0 = 20$, $q_0 = 1$, $a = 1$, $b = 0$.

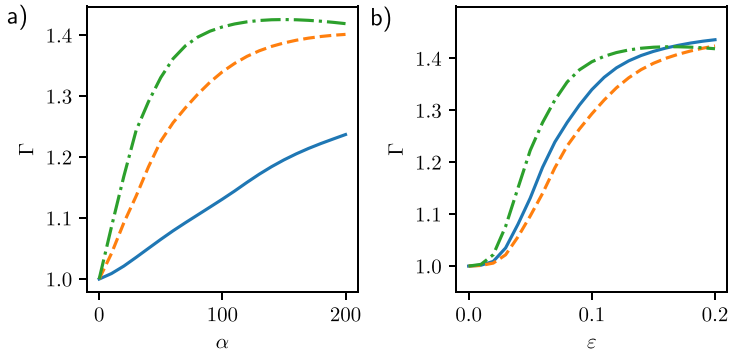

Figure A2. Panel (a) shows the aspect ratio Γ of stationary solutions of equation (A.2) for $a = 1, b = 0$ as a function of the coupling strength α for $\varepsilon = 0.05$ (blue), $\varepsilon = 0.1$ (orange) and $\varepsilon = 0.15$ (green). In (b) Γ is given for a fixed coupling strength $\alpha = 10$ as a function of the control parameter ε for $a = 1, b = 0$ (blue), $a = 1, b = 1$ (orange) and $a = \frac{1}{3}$, $b = 1$ (green). Other parameters as in figure A1.

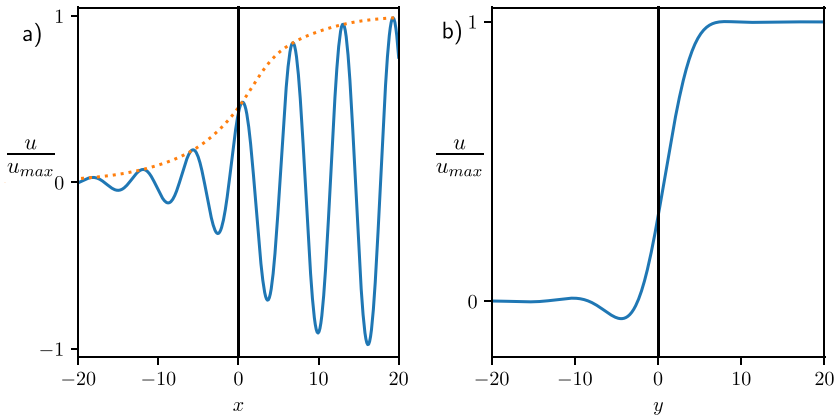

Figure B1. Shown is a stripe pattern as obtained from simulations of equation (10) with **q** perpendicular to the boundary in part (a) and parallel in part (b). The vertical lines mark the domain boundary at $\rho = 0.5$. The red dotted line in (a) describes the x-dependence of the envelope $A(X)$ and the blue line in (b) the envelope $A(Y)$. Parameters: $a = 1, b = 0, \varepsilon = 0.1, D_\rho = 1$.

Appendix B. Decay lengths of the amplitude

The explicit form of the NWSE (3) is given by

$$\tau_0 \partial_t A = \varepsilon A - \xi_0^2 \left(\partial_x - \frac{\mathrm{i}}{2q_0} \partial_y^2 \right)^2 A - g|A|^2 A. \tag{B.1}$$

By rescaling the spatial coordinate x resp. y by the lengths l_n resp. l_p given by equation (B.1) as well as time and amplitude, the coefficients in equation (B.1) become all '1'. For the parameters $q_0 = 1$ and $\varepsilon = 0.1$ the length scale $l_p \simeq 1.78$ for stripes perpendicular to the boundary (i.e. **q** parallel to the boundary) is smaller

than parallel to it with $l_n \simeq 6.32$. This results in different decay lengths of a stripe pattern parallel or perpendicular to a boundary with a control parameter drop as illustrated by a simulation of equation (10) for the parameter set in figure B1.

ORCID iDs

Falko Ziebert https://orcid.org/0000-0001-6332-7287
Walter Zimmermann https://orcid.org/0000-0001-7826-4629

References

[1] Ball P 1998 *The Self-Made Tapestry: Pattern Formation in Nature* (Oxford: Oxford University Press)
[2] Cross M C and Greenside H 2009 *Pattern Formation and Dynamics in Nonequilibrium Systems* (Cambridge: Cambridge University Press)
[3] Meron E 2015 *Nonlinear Physics of Ecosystems* (Boca Raton, FL: CRC Press)
Meron E 2019 *Phys. Today* **72** 30
[4] Lappa M 2009 *Thermal Convection: Patterns, Evolution and Stability* (New York: Wiley)
[5] Cross M C and Hohenberg P C 1993 *Rev. Mod. Phys.* **65** 851
[6] Bodenschatz E, Zimmermann W and Kramer L 1988 *J. Phys.* **49** 1875
[7] Kramer L and Pesch W 1995 *Annu. Rev. Fluid Mech.* **27** 515
[8] Kudrolli A and Gollub J P 1996 *Physica* D **97** 133
[9] St Johnston D and Nüsslein-Volhard C 1992 *Cell* **68** 201
[10] Kondo S and Miura T 2010 *Science* **329** 1616
[11] Loose M, Fischer-Friedrich E, Ries J, Kruse K and Schwille P 2008 *Science* **320** 789
[12] Edelstein-Keshet L, Holmes W R, Zajak M and Dutot M 2013 *Philos. Trans. R. Soc.*, B **368** 20130003
[13] Bergmann F, Rapp L and Zimmermann W 2018 *Phys. Rev.* E **98** 072001(R)
[14] Bergmann F and Zimmermann W 2019 *PLOS ONE* **14** e0218328
[15] Pucci G, Fort E, Amar M B and Couder Y 2011 *Phys. Rev. Lett.* **106** 024503
[16] Hemmerle A, Froehlicher G, Bergeron V, Charitat T and Farago J 2015 *Europhys. Lett.* **111** 24003
[17] Mietke A, Jülicher F and Sbalzarini I F 2019 *Proc. Natl Acad. Sci. USA* **116** 29
[18] Kramer L and Hohenberg P C 1984 *Physica* D **13** 352
[19] Greenside H and Coughran W M 1984 *Phys. Rev.* A **30** 398
[20] Cross M C, Daniels P G, Hohenberg P C and Siggia E D 1983 *J. Fluid Mech.* **55** 155
[21] Cross M C 1982 *Phys. Fluids* **25** 936
[22] Bajaj K M, Mukolobwiez N, Currier N and Ahlers G 1999 *Phys. Rev. Lett.* **83** 5282
[23] Chiam K H, Paul M R, Cross M C and Greenside H 2003 *Phys. Rev.* E **67** 056206
[24] Munuzuri A P, Dolnik M, Zhabotinsky A M and Epstein I R 1999 *J. Am. Chem. Soc.* **121** 8065
[25] Schweizer J, Loose M, Bonny M, Kruse K, Mönch I and Schwille P 2012 *Proc. Natl Acad. Sci. USA* **109** 15283
[26] Kramer L, Ben-Jacob E, Brand H and Cross M C 1982 *Phys. Rev. Lett.* **49** 1891
[27] Cannell D S, Dominguez-Lerma M A and Ahlers G 1983 *Phys. Rev. Lett.* **50** 1365
[28] Riecke H and Paap H G 1987 *Phys. Rev. Lett.* **59** 2570
[29] Cross M C 1984 *Phys. Rev.* A **29** 391
[30] Riecke H and Paap H G 1986 *Phys. Rev.* A **33** 547
[31] Rapp L, Bergmann F and Zimmermann W 2016 *Europhys. Lett.* **113** 28006
[32] Pototsky A and Bestehorn M 2018 *Europhys. Lett.* **121** 46001
[33] Gross P, Kumar K V and Grill S W 2017 *Annu. Rev. Biophys.* **46** 337
[34] Swift J B and Hohenberg P C 1977 *Phys. Rev.* A **15** 319
[35] Bodenschatz E, Pesch W and Ahlers G 2000 *Annu. Rev. Fluid Mech.* **32** 709
[36] Newell A C and Whitehead J A 1969 *J. Fluid Mech.* **38** 279
[37] Karma A and Rappel W J 1998 *Phys. Rev.* E **57** 4323
[38] Emmerich H 2008 *Adv. Phys.* **57** 1
[39] Ziebert F and Aranson I S 2016 *npj Comput. Mater.* **2** 16019
[40] Biben T and Misbah C 2003 *Phys. Rev.* E **67** 031908
[41] Ziebert F, Swaminathan S and Aranson I S 2012 *J. R. Soc. Interface* **9** 1084
[42] Winkler B, Aranson I S and Ziebert F 2016 *Physica* D **318** 26
[43] de Gennes P G and Prost J 1993 *The Physics of Liquid Crystals* (Oxford: Clarendon)
[44] Folch R, Casademunt J, Hernandez-Machado A and Ramirez-Piscina L 1999 *Phys. Rev.* E **60** 1724
[45] Lowe M and Gollub J P 1985 *Phys. Rev.* A **31** 3893
[46] Kramer L and Zimmermann W 1985 *Physica* D **16** 221
[47] Dominguez-Lerma M A, Cannell D S and Ahlers G 1986 *Phys. Rev.* A **34** 4956
[48] Bergmann F, Rapp L and Zimmermann W 2018 *New J. Phys.* **20** 072001
[49] Avery M, Goh R, Goodloe O, Milewski A and Scheel A 2019 *SIAM J. Appl. Dyn. Syst.* **18** 1078
[50] Raskin D M and de Boer P A J 1999 *Proc. Natl Acad. Sci. USA* **96** 4971
[51] Murray S M and Sourjik V 2017 *Nat. Phys.* **13** 1006